SUPPLEMENTARY MATERIAL: Jiang et al. Storm-driven variations in depositional environments modify pyrite sulfur isotope records

1. Supplementary methods

1.1. Sediment sampling

The sediment core SE3 was drilled by rotary drilling with nearly 100% recovery and approximately 64 m in length and split in the laboratory. Before sampling, the core was photographed and described in detail. In this study, we focus on dark gray muddy sediments, which are ideal for organic geochemistry analysis. The muddy sediments are roughly 29 m in length and were stored in refrigerators at 4 °C. A total of 61 samples were collected from the core, at depths from 18.31 to 51.32 m. In detail, 13, 4, 10 and 34 representative muddy samples were collected from the deposits of the floodplain and channel, paleo-estuary, the suspected storm event and offshore shallow-marine facies at intervals of 26 to 259 cm (avg = 84 cm), 9 to 64 cm (avg = 41.5 cm), 1 to 12 cm (avg = 7 cm) and 13 to 130 cm (avg = 60 cm), respectively. The sampling interval varies according to lithological variability. The sediment samples were freeze-dried right after sampling and ground to powders immediately. The powder was divided into several aliquots.

1.2. TS, TC, and TOC measurements

Sixty-one sediment samples were dried for 24 hours at 50 ℃ in a regular oven and ground into powder through a <74 μm sieve and homogenized using a vibratory disc mill (RS200, Retsch, Germany). The powder was divided into several aliquots. The total sulfur (TS) and total carbon (TC) of the sediment samples were determined using a CS-230 C/S analyzer (LECO Corporation,

USA) and this instrument was also used to measure the total organic carbon (TOC) of samples after decarbonation by the method described in Jiang et al. (2021). The relative standard deviations of the TS, TC, and TOC values were less than 5%.

1.3. GC-MS analysis of the saturated hydrocarbon

Gas chromatography-mass spectrometry (GC-MS) analysis of the saturated hydrocarbon fraction in the sediment samples was detailed in Jiang et al. (2019). Briefly, powdered samples (ca. 35 g) were Soxhlet extracted for 72 h using a mixture of dichloromethane (DCM) and methanol (97:3, v/v). The chloroform bitumen A was obtained and purified by asphaltene precipitation with hexane. The hexane was used to elute the saturated hydrocarbon from the extracts using silica/alumina column chromatography. GC-MS analysis of the saturated hydrocarbon fractions was conducted on an Agilent 7890-5975c system (Agilent Technologies, USA) equipped with an HP-5 MS capillary column (60 m × 0.25 mm × 0.25 μm). The *n*-alkanes, pristane (Pr) and phytane (Ph) were identified by comparing their mass spectra and retention indices from literature data (e.g., Peters et al., 2005). The CPI_{long}, TAR and Pr/Ph ratios were calculated from the peak areas in the appropriate molecular ion chromatograms. Samples T10 and T38 were randomly selected for reproducibility analyses (n=3), and the precision was ±0.02 (1SD) for the Pr/Ph ratios.

1.4. Bulk organic carbon isotopic composition

An approximately 250 mg powder sample was decarbonated using excess HCl (2 N) at room temperature in a polypropylene centrifuge tube for 24 hours. After this, the supernatant was removed, and the samples were acidified again with excess HCl (2 N) for 2 hours at 80 °C to confirm the complete removal of carbonates.

The residues were neutralized using deionized water (confirmed by using litmus paper), centrifuged, and dried at 60 °C for 12 hours. Powdered samples (5~25 mg depending on organic matter content) were then loaded into capsules and flash–combusted at 980 °C in a Flash 2000 Elemental Analyzer (Thermo Scientific, UK) fitted with a zero-blank autosampler. The resulting CO_2 was transferred by a ConFlo IV interface for isotopic ratio determination on a Delta V isotope ratio mass spectrometer (Thermo Fisher Scientific, Germany) at the Experimental Technologies Center of Nanjing Institute of Geology and Palaeontology, Nanjing, China. The $\delta^{13}C_{org}$ values are expressed in standard delta notation as per mil (‰) deviations from the Vienna Pee Dee Belemnite (VPDB). Three reference materials were used: USGS42 (–21.09 ± 0.10‰), B2151 (–26.27 ± 0.15‰), and GBW04407 (–22.43 ± 0.07‰), and the analytical precision was better than 0.1‰.

1.5. Stable carbon and oxygen isotopic compositions of carbonates

The stable carbon ($\delta^{13}C$) and oxygen ($\delta^{18}O$) isotopic composition in carbonates of the powdered samples (~0.1 g) were measured with a Finnigan Delta Plus XP stable isotope mass spectrometer (Thermo Finnigan, Germany) coupled with the Gas Bench II online sample preparation device (Thermo Finnigan, Germany) at the State Key Laboratory for Mineral Deposits Research, Nanjing University, China. The powder reacted with orthophosphoric acid for >12 hours at 70 ℃ in Gas Bench II to generate CO_2, which was then transferred to and measured in Finnigan Delta Plus XP according to Li et al. (2019). Chinese national carbonate standards (GBW04405) TTB-1 (calcite) and TTB-2 (dolomite) were analyzed for two-point isotope ratio normalization. Both the carbon and oxygen isotopic ratios were normalized to Vienna PDB in δ notation. The internal precision was better than ± 0.09‰ and ± 0.08‰ (1SD)

for $\delta^{13}C$ and $\delta^{18}O$, respectively, and the external reproducibility was better than ± 0.5‰ for both $\delta^{13}C$ and $\delta^{18}O$.

1.6. Stable carbon and oxygen isotopic compositions of shells

The stable carbon ($\delta^{13}C$) and oxygen ($\delta^{18}O$) isotopic composition in Corbicula fluminea shells were measured with the Kiel IV–MAT 253 system (Thermo Fisher Scientific, Bremen, Germany) at the Experimental Technologies Center of Nanjing Institute of Geology and Palaeontology, Nanjing, China. Analytical precision was better than 0.02‰ for $\delta^{13}C$ (VPDB) and 0.04‰ for $\delta^{18}O$ (VPDB). The experimental processes followed those reported in Wang et al. (2020).

1.7. Sr abundance

Sr abundance was analyzed in solution using a Finnigan Element II mass spectrometer (Thermo Fisher Sci., USA) at the State Key Laboratory for Mineral Deposits Research, Nanjing University, Nanjing, China. The repeated analysis of in-run check standards was better than 5%. The detailed analytical procedure has been reported in Zhang et al. (2018).

1.8. AMS-^{14}C dating

The chronology was established using four plant or shell samples (Fig. 1C). Radiocarbon dating of given samples from the core SE3 was performed by accelerator mass spectrometry (AMS) at the Beta Analytic, Miami, Florida, USA. The dating results were obtained by measuring sample $^{14}C/^{13}C$ relative to the $^{14}C/^{13}C$ in Oxalic Acid II (NIST-4990C) in a particle accelerator using an SNICS ion source. The calendar age ranges (1σ, cal yr BP) were calibrated

with BetaCal 3.21 using the IntCal 13 atmospheric calibration curve. The ages are expressed in years before the present (BP), where “present” is defined as 1950 C.E. The measured and calibrated ages were given in Table S1.

Supplementary figures

Figure S1. Photo of the selected paleo–estuary and offshore shallow marine sediments from the core SE3, which are characterized by light gray and relatively homogeneous deposits compared with the muddy storm deposit. (A) Photo of the paleo-estuary sediment (depth at 40.0 to 40.8 m). (B) Photo of the offshore shallow marine sediment (depth at 37.2 to 38.0 m).

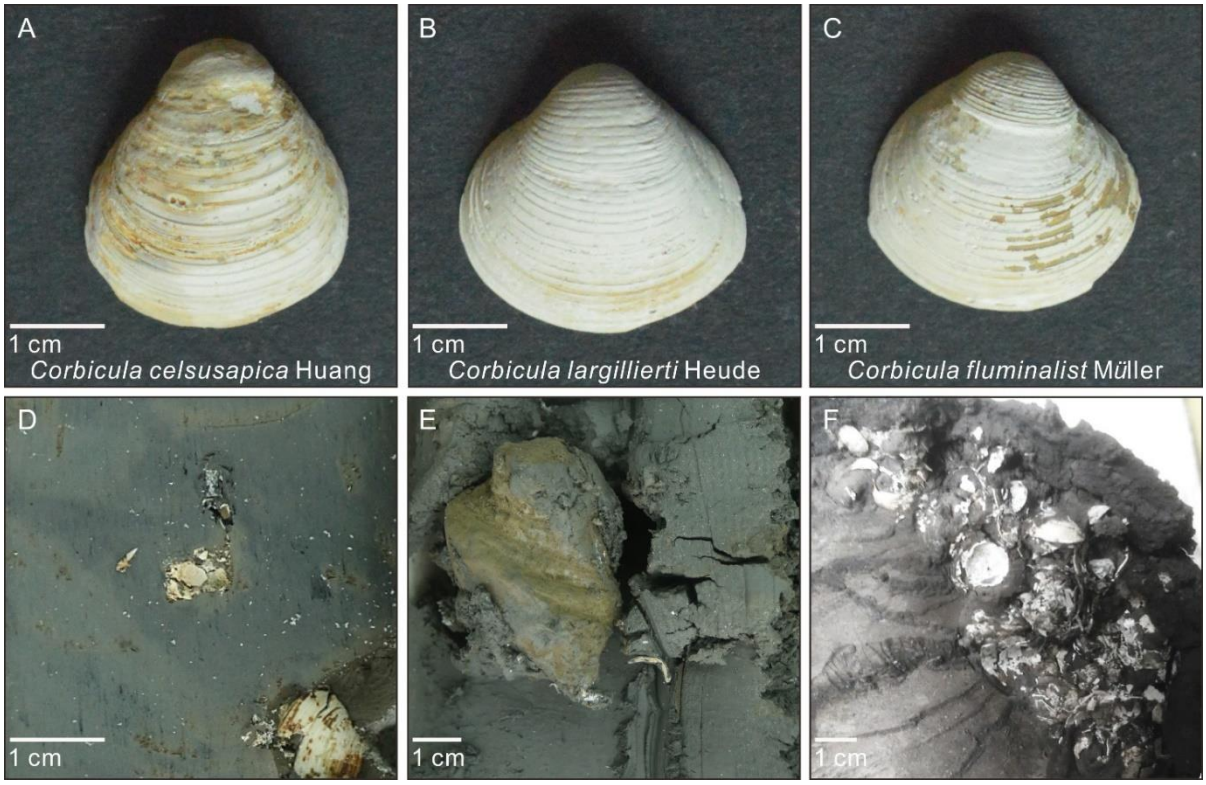

Figure S2. Sediment compositions of the muddy storm deposit in the core SE3. (A–C) mollusk shells found in the high-energy storm peak phase (in samples T40 and T41). They were most likely derived from the underlying paleo-estuarine sediments, formed by storm-induced resuspension and redeposition. (D) Sediment mixing of gray mud, and grayish-yellow siliciclastic silt in the muddy storm deposit (~39.35 m) indicating high-energy storm peak phase. (E) The largest muddy gravel found in the muddy storm deposit (~39.03 m) in the high-energy storm peak phase. (F) Shell fragments accumulation formed by storm-induced resuspension and redeposition (~39.10 m).

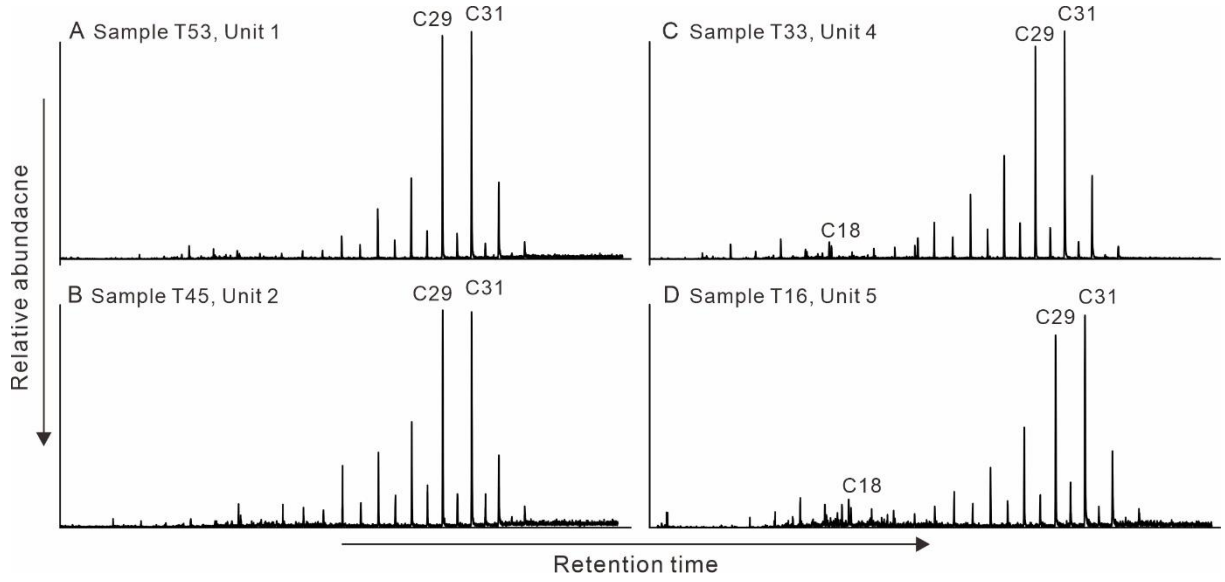

Figure S3. Mass chromatograms of m/z 85 depicting typical unimodal distributions of *n*-alkanes in selected sediment samples. (A) Sample T53 obtained from unit 1. (B) Sample T45 obtained from unit 2. (C) Sample T33 obtained from unit 4. (D) Sample T16 obtained from unit 5. Numbers over the peaks identify individual carbon number *n*-alkanes.

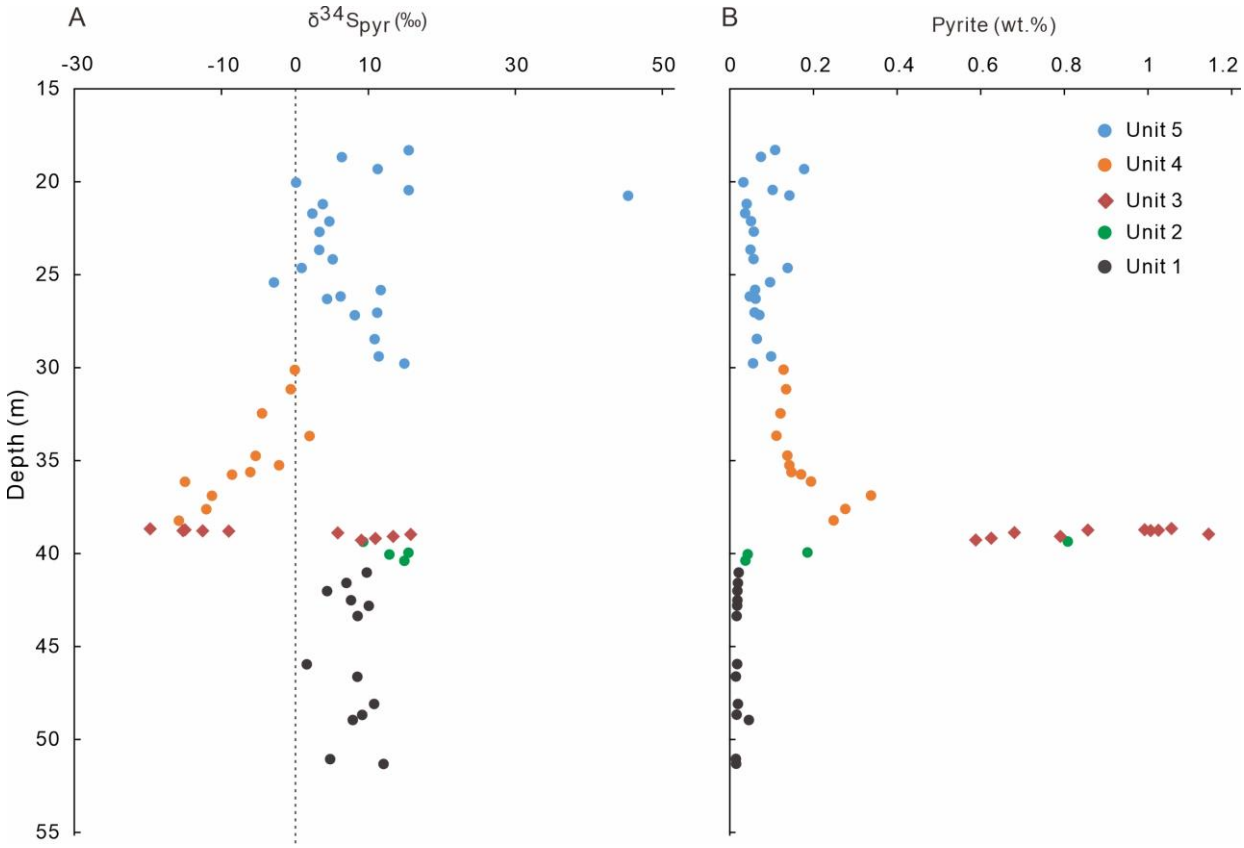

Figure S4. Depth profiles of sulfur isotopic compositions of pyrite (A) and pyrite contents (B). Note that the depth axis is linear (cf. Fig. 2).

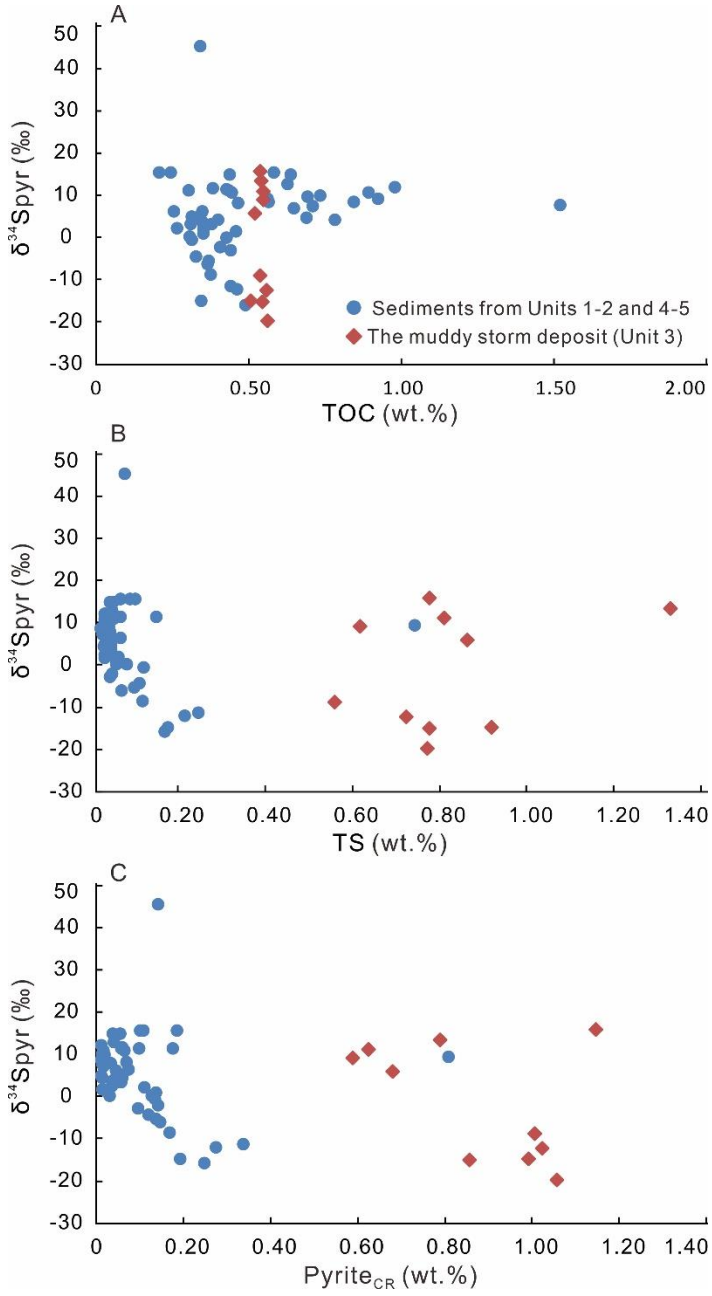

Figure S5. (A) $\delta^{34}S_{pyr}$ value versus TOC content in the same sediment samples; (B) $\delta^{34}S_{pyr}$ value versus total sulfur content in the same sediment samples; (C) $\delta^{34}S_{pyr}$ value versus content of pyrite determined by CRS extraction in the same sediment samples.

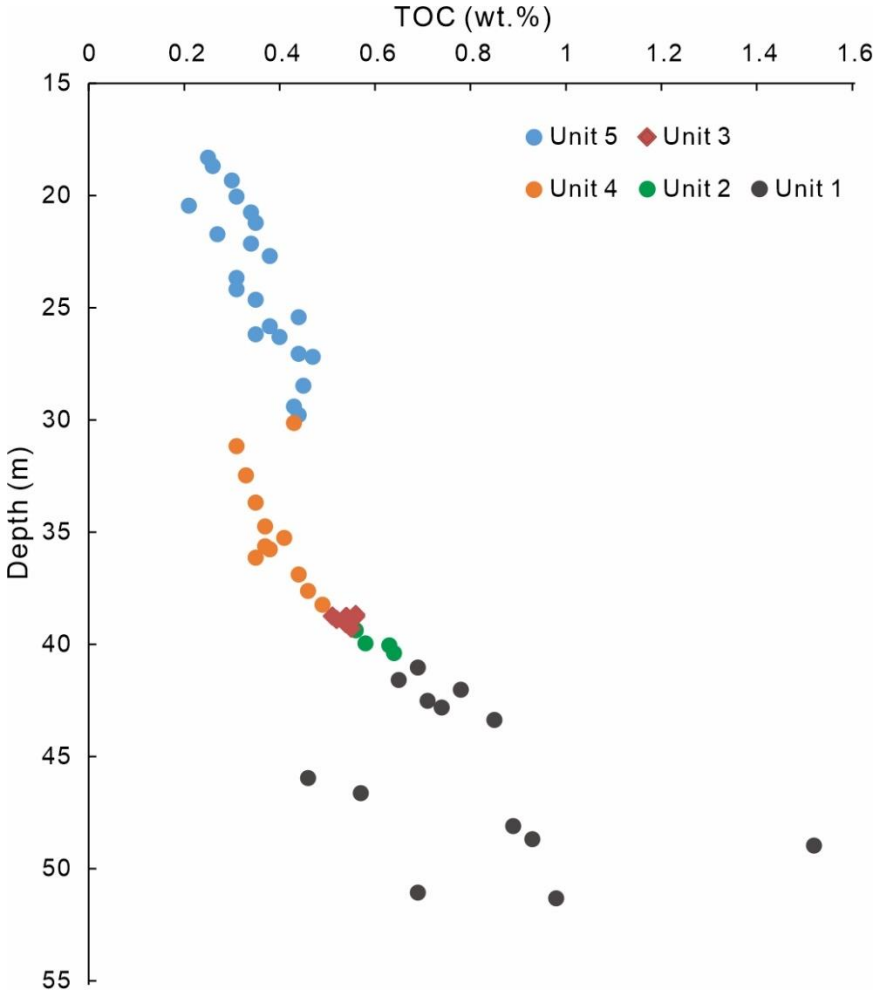

Figure S6. Total organic carbon (TOC) contents versus depth plot.

Supplementary tables

Table S1. Radiocarbon dating results of sediments from core SE3 in the Qiantang River incised valley.

Lab ID	Sample No.	Depth (m)	Material	$\delta^{13}C_{organic}$ (‰, VPDB)	Conventional Age (1σ, yr BP)	Calibrated Age (1σ, cal yr BP)
Beta – 517519	SE303	18.92	Plant material	– 26.5	7220 ± 30	8016 ± 51
Beta – 517520	SE307	29.9	Shell	– 4.3	8650 ± 30	9609 ± 67 [a]
Beta – 517521	SE310	36.43	Wood	– 28.7	7780 ± 30	8558 ± 51
Beta – 517522	SE313	44.00 ~ 44.05	Shell	– 2.1	8230 ± 30	9194 ± 107
Beta – 517523	SE315	50.72 ~ 50.80	Plant material	– 27.1	8290 ± 30	9313 ± 111

Note: superscript "a" indicates that the AMS-^{14}C dating of this sample was not adopted in this study, due to the abnormally old AMS-derived age.

Table S2. Geochemical data of muddy sediments from core SE3.

Sample ID	Depth (m)	TOC (wt.%)	TC (wt.%)	Carbonate (wt.%)	TS (wt.%)	TOC /S_{pyr}	Sr ($\mu g.g^{-1}$)	$\delta^{13}C_{org}$ (‰)	CPI_{long}	Pr/Ph	TAR	Pyrite (wt.%)	$\delta^{34}S_{pyr}$	$\Delta\delta^{34}S$	$\delta^{13}C_{TIC}$ (‰)	$\delta^{18}O_{TIC}$ (‰)
Unit 5																
T1	18.31	0.25	0.70	0.45	0.08	4.34	152.34	-25.01	2.38	0.67	10.75	0.108	15.5	5.5	-0.54	-8.21
T2	18.68	0.26	0.83	0.57	0.05	6.59	152.21	-24.47	1.93	0.74	1.04	0.074	6.4	14.6	-0.95	-8.20
T3	19.33	0.30	0.93	0.63	0.14	3.18	143.70	-24.00	3.59	0.72	12.83	0.177	11.3	9.7	-1.45	-7.87
T4	20.05	0.31	0.94	0.63	0.05	18.18	151.72	-23.86	4.21	0.71	11.61	0.032	0.2	20.8	-1.27	-7.72
T5	20.46	0.21	0.84	0.63	0.06	3.86	155.84	-24.33	2.78	0.17	8.98	0.102	15.5	5.5	-0.84	-8.06
T6	20.76	0.34	0.96	0.62	0.06	4.49	143.99	-24.30	4.61	0.54	21.74	0.142	45.3	-24.3	-1.28	-7.73
T7	21.21	0.35	1.04	0.69	0.03	16.42	143.78	-24.63	4.37	0.70	7.92	0.040	3.8	17.2	-1.30	-8.05
T8	21.72	0.27	0.77	0.50	0.02	14.07	154.65	-23.98	3.12	0.66	2.41	0.036	2.4	18.6	-1.23	-8.21
T9	22.14	0.34	1.06	0.72	0.03	12.76	147.08	-23.78	4.55	0.79	10.69	0.050	4.7	16.3	-1.36	-8.34
T10	22.70	0.38	0.97	0.59	0.03	12.51	72.15	-23.79	4.16	0.68	9.74	0.057	3.3	17.7	-1.37	-8.00
T11	23.67	0.31	0.99	0.68	0.03	11.87	160.59	-24.11	3.77	0.49	16.66	0.049	3.3	17.7	-1.00	-7.84
T12	24.18	0.31	0.82	0.51	0.02	10.39	154.97	-24.43	3.85	0.64	13.92	0.056	5.1	15.9	-0.53	-8.15
T13	24.65	0.35	0.75	0.40	0.05	4.76	13.04	-23.69	4.21	0.63	10.66	0.138	0.9	20.1	-0.78	-7.91
T14	25.42	0.44	0.69	0.25	0.03	8.6	119.51	-23.39	4.17	0.55	21.01	0.096	-2.9	23.9	-1.22	-7.64
T15	25.83	0.38	0.85	0.47	0.03	11.88	113.92	-24.15	4.45	0.38	34.20	0.060	11.7	9.3	-1.68	-7.89
T16	26.18	0.35	0.90	0.55	0.03	13.97	130.24	-24.37	4.01	0.60	17.22	0.047	6.2	14.8	-1.13	-7.97
T17	26.31	0.40	0.84	0.44	0.02	12.3	134.31	-23.71	4.36	0.56	13.32	0.061	4.4	16.6	-1.38	-7.81
T18	27.05	0.44	0.96	0.52	0.05	13.99	130.99	-23.54	4.92	0.64	15.12	0.059	11.2	9.8	-1.32	-7.87
T19	27.19	0.47	0.84	0.37	0.02	12.6	114.28	-24.16	3.83	0.59	9.06	0.070	8.2	12.8	-2.15	-7.38
T20	28.47	0.45	0.93	0.48	0.04	13.19	126.76	-23.47	4.32	0.71	14.48	0.064	10.8	10.2	-1.42	-7.67
T21	29.41	0.43	0.92	0.49	0.06	8.23	124.43	-23.41	4.59	0.47	34.20	0.098	11.4	9.6	-1.57	-7.56
T22	29.78	0.44	0.90	0.46	0.04	15.01	122.73	-23.97	4.46	0.47	32.67	0.055	14.9	6.1	-1.86	-7.70
Unit 4																
T23	30.13	0.43	0.83	0.40	0.07	6.3	128.09	-23.27	4.08	0.59	14.83	0.128	0	21.0	-0.87	-7.92
T24	31.17	0.31	0.67	0.36	0.11	4.34	120.82	-24.10	3.49	0.59	14.01	0.134	-0.6	21.6	-0.30	-8.27
T25	32.47	0.33	0.67	0.34	0.10	5.12	125.41	-24.05	3.38	0.46	11.31	0.121	-4.5	25.5	-0.76	-7.81
T26	33.68	0.35	0.65	0.30	0.05	5.92	121.19	-23.87	4.04	0.58	20.29	0.111	2.0	19.0	-0.62	-7.83

T27	34.75	0.37	0.60	0.23	0.09	5.07	110.40	-24.28	3.53	0.56	11.44	0.137	-5.4	26.4	-0.71	-7.80
T28	35.26	0.41	0.45	0.04	0.04	5.42	108.68	-23.32	4.25	0.76	12.48	0.142	-2.2	23.2	–	–
T29	35.63	0.37	0.47	0.10	0.06	4.72	109.68	-24.09	3.18	0.61	8.98	0.147	-6.1	27.1	-0.38	-7.34
T30	35.76	0.38	0.56	0.18	0.11	4.19	107.43	-24.53	4.06	0.75	10.72	0.170	-8.6	29.6	-0.11	-7.39
T31	36.14	0.35	0.47	0.12	0.16	3.38	98.48	-24.51	3.06	0.74	7.95	0.194	-15.0	36.0	-0.51	-7.72
T32	36.89	0.44	0.53	0.09	0.24	2.45	91.43	-24.65	3.64	0.74	9.59	0.337	-11.3	32.3	–	–
T33	37.62	0.46	0.53	0.07	0.20	3.13	85.48	-24.53	3.85	0.50	30.82	0.276	-12.1	33.1	–	–
T34	38.23	0.49	0.56	0.07	0.16	3.71	74.65	-25.24	3.11	0.47	22.96	0.248	-15.8	36.8	–	–
Unit 3																
T35	38.67	0.56	0.62	0.06	0.77	0.99	82.82	-25.65	–	–	–	1.056	-19.7	40.7	–	–
T36	38.73	0.51	0.67	0.16	0.92	0.97	/	-25.47	2.26	0.29	3.27	0.991	-15.0	36.0	-1.11	-6.53
T37	38.75	0.54	0.61	0.07	0.78	1.18	/	-25.44	1.76	0.42	1.38	0.856	-15.2	36.2	–	–
T38	38.76	0.56	0.61	0.05	0.72	1.03	/	-25.40	2.21	0.37	2.94	1.023	-12.5	33.5	–	–
T39	38.78	0.54	0.59	0.05	0.56	1.01	/	-25.53	1.94	0.43	1.41	1.006	-9.0	30.0	–	–
T40	38.89	0.52	0.80	0.28	0.86	1.43	/	-25.18	2.38	0.45	2.49	0.680	5.8	15.2	4.84	-4.54
T41	38.97	0.54	0.69	0.15	0.78	0.88	/	-25.37	2.13	0.40	3.49	1.145	15.8	5.2	1.16	-5.67
T42	39.09	0.54	0.61	0.07	1.33	1.28	/	-25.39	2.56	0.52	2.48	0.790	13.4	7.6	–	–
T43	39.19	0.55	0.60	0.05	0.81	1.65	/	-25.31	2.62	0.60	2.12	0.625	11.0	10.1	–	–
T44	39.29	0.55	0.62	0.07	0.62	1.75	/	-25.34	2.67	0.55	1.95	0.588	9.0	12.0	–	–
Unit 2																
T45	39.37	0.56	0.65	0.09	0.74	1.3	71.89	-24.98	3.99	0.40	49.87	0.808	9.3	11.7	–	–
T46	39.96	0.58	0.65	0.07	0.09	5.88	76.01	-25.19	4.96	0.64	20.83	0.185	15.4	5.6	–	–
T47	40.05	0.63	0.80	0.17	0.04	28.14	70.52	-24.90	4.85	0.54	27.58	0.042	12.9	8.2	1.92	-5.88
T48	40.39	0.64	0.71	0.07	0.03	32.45	64.95	-24.60	–	–	–	0.037	14.9	6.1	–	–
Unit 1																
T49	41.03	0.69	0.82	0.13	0.02	143.84	64.49	-25.47	4.04	0.65	22.13	0.009	9.8	11.3	0.88	-8.20
T50	41.59	0.65	0.74	0.09	0.01	174.22	70.31	-25.27	2.62	0.45	72.84	0.007	7.0	14.0	–	–
T51	42.02	0.78	0.88	0.10	0.02	243.9	72.47	-25.41	3.07	0.61	24.56	0.006	4.4	16.6	–	–
T52	42.52	0.71	0.82	0.11	0.02	222.01	70.44	-25.00	5.43	0.59	31.03	0.006	7.6	13.4	–	–
T53	42.81	0.74	0.89	0.15	0.02	277.67	71.01	-24.96	5.42	0.45	57.18	0.005	10.0	11.0	–	–
T54	43.37	0.85	0.95	0.10	0.02	398.69	73.95	-25.35	5.88	0.57	38.80	0.004	8.5	12.5	–	–
T55	45.96	0.46	0.53	0.07	0.02	172.61	63.37	-25.66	5.05	0.44	75.10	0.005	1.6	19.4	–	–
T56	46.63	0.57	0.56	0.00	0.01	534.71	67.14	-25.35	5.49	0.36	111.43	0.002	8.5	12.5	–	–

T57	48.10	0.89	1.00	0.11	0.02	238.54	125.86	-25.34	5.40	0.45	74.62	0.007	10.8	10.2	3.21	-7.05
T58	48.68	0.93	0.99	0.06	0.03	436.21	69.85	-25.01	5.38	0.53	38.35	0.004	9.1	11.9	–	–
T59	48.96	1.52	1.60	0.08	0.03	86.42	71.37	-26.61	6.43	0.57	31.60	0.033	7.9	13.1	–	–
T60	51.06	0.69	0.89	0.20	0.02	647.28	58.53	-25.55	4.65	0.55	28.78	0.002	4.8	16.2	0.63	-7.47
T61	51.32	0.98	1.10	0.12	0.02	612.88	66.34	-25.61	6.32	0.55	63.12	0.003	12.0	9.0	1.39	-7.83

Note: "–" and "/" indicate below the detection limit and not determined, respectively. $\Delta\delta^{34}S = \delta^{34}S_{\text{seawater sulfate}} - \delta^{34}S_{\text{sulfide}}$, where $\delta^{34}S_{\text{seawater sulfate}} = +21‰$.

References

Jiang, K., Lin, C., Guan, C., Peng, L., Zhang, X., Cai, C., Xiao, Q., Huang, S., 2021. Influence of a chromium reduction treatment in the analysis of organic carbon isotopes in Quaternary coastal plain incised valley sediments. Appl. Geochem. 127, 104922. https://doi.org/10.1016/j.apgeochem.2021.104922.

Jiang, K., Lin, C., Peng, L., Zhang, X., Cai, C., 2019. Methyltrimethyltridecylchromans (MTTCs) in lacustrine sediments in the northern Bohai Bay Basin, China: Org. Geochem. 133, 1–9. https://doi.org/10.1016/j.orggeochem.2019.03.003.

Li, W., Bialik, O.M., Wang, X., Yang, T., Hu, Z., Huang, Q., Zhao, S., Waldmann, N.D., 2019. Effects of early diagenesis on Mg isotopes in dolomite: The roles of Mn (IV)–reduction and recrystallization. Geochim. Cosmochim. Acta 250, 1–17. https://doi.org/10.1016/j.gca.2019.01.029.

Peters, K.E., Walters, C.C., Moldowan, J.M., 2005. The Biomarker Guide, Biomarkers and Isotopes in Petroleum Exploration and Earth History. Cambridge University Press, Cambridge, 1155 p.

Wang, W.Q., Garbelli, C., Zhang, F.F., Zheng, Q.F., Zhang, Y.C., Yuan, D.X., Shi, Y.K., Chen, B., Shen, S.Z., 2020. A high–resolution Middle to Late Permian paleotemperature curve reconstructed using oxygen isotopes of well–preserved brachiopod shells. Earth Planet. Sci. Lett. 540, 116245. https://doi.org/10.1016/j.epsl.2020.116245.

Zhang, B., Yao, S., Wignall, P.B., Hu, W., Ding, H., Liu, B., Ren, Y., 2018. Widespread coastal upwelling along the Eastern Paleo–Tethys Margin (South China) during the Middle Permian (Guadalupian): implications for organic matter accumulation. Mar. Pet. Geol. 97, 113–126. https://doi.org/10.1016/j.marpetgeo.2018.06.025.